



Degradation of ciprofloxacin by UV and UV/H₂O₂ via multiple-wavelength ultraviolet light-emitting diodes: Effectiveness, intermediates and antibacterial activity

Hua-se Ou^a, Jin-shao Ye^{a,*}, Sheng Ma^a, Chao-hai Wei^b, Nai-yun Gao^c, Jia-zhao He^a

^a Guangzhou Key Laboratory of Environmental Exposure and Health, School of Environment, Jinan University, Guangzhou 510632, PR China

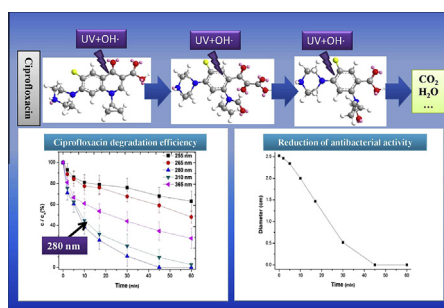
^b The Key Lab of Pollution Control and Ecosystem Restoration in Industry Clusters, Ministry of Education, School of Environment and Energy, South China University of Technology, Guangzhou Higher Education Mega Centre, Guangzhou 510006, PR China

^c State Key Laboratory of Pollution Control and Resources Reuse, College of Environmental Science and Engineering, Tongji University, Shanghai 200092, PR China

HIGHLIGHTS

- Ciprofloxacin is degraded by UV and UV/H₂O₂ via multiple wavelengths UV-LEDs.
- 280 nm UV-LED/H₂O₂ has the highest efficiency for ciprofloxacin degradation.
- UV irradiation only induces transformations of peripheral functional groups.
- UV/H₂O₂ induces consecutive oxidation of core quinolone functional group.
- Incomplete degradation of ciprofloxacin reduced its antibacterial activity.

GRAPHICAL ABSTRACT



ARTICLE INFO

Article history:

Received 13 October 2015

Received in revised form 3 January 2016

Accepted 5 January 2016

Available online 8 January 2016

Keywords:

Ultraviolet light-emitting diode
Antibiotic
Photolysis
Photocatalysis
Water treatment

ABSTRACT

Although the efficiency and mechanism of the degradation of quinolone antibiotics by 254 nm UV radiation or UV/H₂O₂ have been well elucidated, the same is not true for other UV wavelengths. The degradation of ciprofloxacin (CIP), a representative quinolone, was explored by UV and UV/H₂O₂ using 255, 265, 280, 310 and 365 nm ultraviolet light-emitting diodes (UV-LEDs). The results of LC/MS² indicated that treatment at 280 nm UV/H₂O₂ had the highest removal efficiency ([CIP] = 30 μM, apparent rate constants reached 0.0759 min⁻¹, half-time at 9.1 min) among these five wavelengths. Both the qualitative and quantitative analyses demonstrated that the intermediate abundance and distribution at 280 nm UV/H₂O₂ were drastically altered in comparison to traditional 254 nm UV irradiation or photocatalysis. In the 280 nm UV-LED irradiation experiment, the primary intermediate was C₁₇H₁₉N₃O₄ (*m/z* 330.1), which was generated by the substitution of the fluorine by a hydroxyl. In the 280 nm UV-LED/H₂O₂ experiment, the dominant intermediate was C₁₇H₁₈FN₃O₄ (*m/z* 348.1), in which a hydroxyl was added at the C=C bond of the cyclohexene moiety. The further oxidation of C₁₇H₁₈FN₃O₄ was proposed to involve a consecutive oxidation pathway, following the order of CIP, C₁₇H₁₈FN₃O₄, C₁₇H₁₈FN₃O₅, C₁₆H₁₈FN₃O₄ and C₁₅H₁₈FN₃O₃, which eventually destroyed the quinolone structure. Notably, the microbial analysis also proved that 280 nm UV-LED/H₂O₂ degraded the moieties those are responsible for antibacterial activity. Based on these results, it was concluded that 280 nm UV-LED/H₂O₂ can be used as a novel effective technology to improve the removal efficiency of quinolones in wastewater treatment.

© 2016 Elsevier B.V. All rights reserved.

* Corresponding author at: Room 457, The Second Science and Technology Building, Jinan University, 601 Huangpu Avenue West, Guangzhou 510632, PR China. Tel.: +86 20 85226615.

E-mail address: jsye@jnu.edu.cn (J.-s. Ye).

1. Introduction

Quinolones are synthetic antibiotics that are widely used throughout the world as human and veterinary medicines. Quinolones are not biodegradable, and this feature results in their incomplete degradation in conventional biological wastewater treatment plants; therefore, residues of quinolones and their derivatives were discharged and detected in natural water bodies [1,2]. In recent years, many studies have confirmed that the existence of quinolones in the environment causes severe problems, including the induction of antibiotic resistance [3], the physiological teratogenesis of plants and algae [4], and the genotoxicity/carcinogenic potential [5]. In view of these facts, researchers are making efforts to develop cost-effective non-biological treatment methods to eliminate quinolones.

The popular advanced oxidation processes (AOPs), including Fenton oxidation [6], ozonation [7], peroxymonosulfate oxidation [8] and photocatalysis [9], were all shown to be effective for quinolones. Among these technologies, photolysis/photocatalysis using UV or visible light is very attractive because of its low cost, reduced use of chemicals, simple operation and wide application against a wide range of environmental pollutants. The decomposition of quinolones induced by UV photolysis was verified, but its mineralization rate was relatively low [10]. In contrast, photocatalysis using UV/visible light combined with catalysts generates hydroxyl radicals (OH[•]); thus, it has shown to lead to nonselective oxidation of quinolones, and its mineralization rate was higher [11–13].

Although multiple catalysts were developed and proven to be effective, the existing literature regarding the photolysis and photocatalysis of quinolones has never considered the optimization of the irradiation wavelength or the light source. Because quinolones are photosensitive molecules, screening for the optimal absorptive UV wavelength may improve its removal efficiency. Unfortunately, most studies have used a mercury arc lamp at a wavelength of 254 nm [14] or a xenon lamp with a continuous spectrum [15]. Moreover, these light sources have some drawbacks, such as high energy consumption, release of toxic heavy metals, frequent lamp replacement and fragility [16]. Thus, the exploration of more efficient UV wavelengths using eco-friendly light sources for the degradation of quinolones is urgently needed.

Within the last decade, the development of production techniques for solid-state devices has provided us with a compact, low-cost, low-energy, and environmentally friendly light-emitting diode (LED). The LED is free of toxicants and emits light at independent narrow bands (half bandwidth < 10 nm) [17]. An ultraviolet LED (UV-LED), which can emit UV light in the range of 200–400 nm, has been developed based on an aluminum gallium nitride material [18]. Thus, UV-LEDs can be used for the screening of the optimal wavelength for the degradation of particular organic contaminants. Recently, multifarious reactors based on UV-LEDs emitting different wavelengths were developed to degrade certain organic indicator compounds, including phenol [19], formaldehyde [20], methylene blue [21], methyl red [22] and even fulvic acids [23]. However, their ability to degrade antibiotics is still unknown.

In the present study, our research group designed a UV-LED module for the experimental degradation of antibiotics. Ciprofloxacin (CIP) was selected as an indicative quinolone, and the effectiveness of direct photolysis as well as UV/H₂O₂ oxidation using UV-LEDs of different wavelengths was evaluated. The structures and generative pathways of the reaction intermediates were elucidated using a high-resolution tandem mass spectrometry. Finally, the reduction of antibacterial activity was evaluated by microbiological analysis. The findings of this study can be used to develop effective non-biological degradation methods for quinolones.

2. Materials and methods

2.1. Chemical reagents

Crystal CIP (98%, HPLC grade) and norfloxacin (98%, HPLC grade) were purchased from Sigma–Aldrich (USA) and stored at 4 °C. Analytical grade Na₂SO₃ (98%) and H₂O₂ (30%, v/v) were purchased from Sinopharm (China). HPLC grade acetonitrile and formic acid were purchased from Merck (Germany). All reagents were used as received. All of the solutions were prepared using ultrapure water (electrical resistivity: 18.2 MΩ) produced by a Milli-Q Advantage A10 system (Millipore, USA).

2.2. UV-LED micro-module

A UV-LED irradiation micro-module was designed and assembled. This module consisted of five components, including a UV-LED array, power source, heat dissipation device, module framework and reactor vessel (Fig. 1). The UV-LED array was composed of a series of UV-LED chips, which had maximum emission peaks at 255, 265, 280, 310 or 365 nm, and the half-wave bandwidth of these chips was 10 nm (Fig. S1). The irradiating intensities of the UV-LEDs were measured using a HAAS-3000 light spectrum irradiation meter (Everfine, China). The average irradiation intensity of the 280 nm UV-LED chips was 0.023 mW cm⁻² at the surface of the reaction solution. The irradiation dose was calculated as:

$$\text{Dose} = \text{Int} \times T \quad (1)$$

where *Int* is the irradiation intensity and *T* is the irradiation time (s), and the irradiation dose has units of mJ cm⁻². The irradiation intensities and doses of UV-LED chips of other wavelengths were also obtained using similar methods. In each array, a total of 16 UV-LED chips were set as a 4 × 4 matrix upon the 6-cm diameter dish, and the dish was placed on the shaker. The arrangements were similar to all of the wavelength experiments. The module framework was designed by AutoCAD (Autodesk, USA) and was produced using the laser rapid prototyping technique. A customized circular quartz vessel (6-cm diameter) was used as the reactor vessel.

2.3. UV-LED irradiation experiments

Twenty milliliters of CIP solution at 10 mg L⁻¹ (30 μM) was spiked into the quartz vessel. In the UV/H₂O₂ experiments, the initial concentration of H₂O₂ was 10.2 mg L⁻¹ (300 μM). The pH value was maintained in the range of 6.5–7.2 using a 5.0 mM phosphate buffer solution. The experiments were performed in a customized incubator with constant temperature control. The solution was maintained at 25 ± 2 °C, and uniformity was achieved by shaking the dish at 60 r min⁻¹. The reaction was initiated by turning on the UV-LED array. At a pre-defined time, Na₂SO₃, at a concentration that was stoichiometrically equivalent to the initial H₂O₂ dose, was added to stop the reaction. Afterwards, 5 mL of the sample was transferred into a brown amber tube and then stored at 4 °C before sample analysis. The H₂O₂-only control experiments were included in the experimental design.

2.4. HPLC separation

Before HPLC separation, all samples were mixed with isometric methanol that contained 1 mg L⁻¹ norfloxacin. The concentrations of CIP and the intermediates were verified by MS analysis using norfloxacin as an internal standard. The samples were injected into a LC-30AD liquid chromatograph system (Shimadzu, Japan) with a Waters Symmetry C-18 column (2.1 × 150 mm, 3.5 μm) prior to the MS analysis. The injection volume was 10 μL, and the mobile

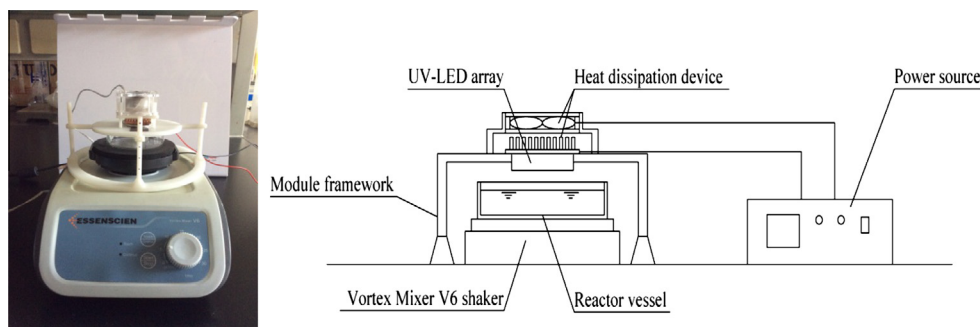


Fig. 1. Micro-UV-LED module and its schematic diagram.

phase was a gradient elution of 0.1% formic acid water solution (mobile phase A) and acetonitrile (mobile phase B). The gradient elution was programmed as follows: 0–3.0 min, 10–90% B; 3.0–7.0 min, 90% B; 7.0–7.1 min, 90–10% B; 7.1–10.0 min, 10% B ($40\text{ }^{\circ}\text{C}$, 0.3 mL min^{-1}).

2.5. Reaction intermediate analysis

The identification of intermediates was performed using a TripleTOF 5600+ high-resolution tandem mass spectrometry (HRMS) (Applied Biosystems SCIEX, USA) equipped with a Turbo V ESI ion source and a triple quadrupole time-of-flight (ToF) device. The instrumentation conditions are listed in Table 1. Nitrogen served both as the turbo and the collision gas. Mass calibrations and resolution adjustments on the quadrupoles and ToF were performed automatically using a 10^{-5} M solution of polypropylene glycol (PPG) introduced via a model II Harvard infusion pump. The scan range was set at m/z 50–600. The data were analyzed using PeakView and MasterView (Applied Biosystems SCIEX, USA). A systematic intermediate screening procedure is discussed in Supporting Information.

2.6. Quantitative analysis of CIP and its intermediates

The quantitative analysis of CIP and its degrading intermediates was performed using a TripleQuad 5500 tandem mass spectrometry (Applied Biosystems SCIEX, USA). Most of the instrumentation conditions were similar to those of the 5600+ system, but the Collision-induced Dissociation (CID) energy was optimized for different intermediates. The scan mode was multi-reaction monitoring (MRM), and the monitoring ion pairs are listed in Table S1.

2.7. Total organic carbon (TOC) and microbial analysis

To evaluate the mineralization efficiency, the TOC was measured using a VCSH-ASI TOC analyzer (Shimazu, Japan). The microbial experiment was performed to evaluate whether the reaction

intermediates retained antibacterial activity. The agar plates were first inoculated with $1.2 \times 10^8\text{ cfu mL}^{-1}$ *Escherichia coli* (ATCC 11303), and parallel $10\text{-}\mu\text{L}$ samples were separately spiked on agar plates. The plates were then incubated at $37\text{ }^{\circ}\text{C}$ for 24 h, and the inhibition halo was measured. The diameter of the inhibition halo represented the antibacterial activity.

2.8. Computational methods of CIP properties

The correlation of the molecular properties of CIP and its potential transformation pathway were computed by ChemBioDraw Ultra version 2015 [24]. Briefly, the molecular structure of CIP was drawn using ChemBioDraw and then copied to ChemBio3D to create a three-dimensional model. Subsequently, the structure was subjected to energy minimization by molecular mechanics until the root-mean-square gradient became smaller than $0.01\text{ kcal mol}^{-1}\text{ \AA}$. The bond energy and bond length of all atoms were calculated from the computed properties.

3. Results and discussion

3.1. Degradation kinetics of CIP

The result of the H_2O_2 -only control experiment is presented in Fig. S2. A slight variation in the CIP concentration was observed, indicating that H_2O_2 had a negligible effect on CIP. The removal effectiveness of the UV-LED-only irradiation experiments is presented in Fig. 2a, while the apparent rate constants and half-times are summarized in Table 2. Illumination at 280 and 310 nm resulted in significant removal of the CIP, but the other wavelengths only induced slight variations. For 10 mg L^{-1} ($30\text{ }\mu\text{M}$) CIP, the highest removal effectiveness reached $\sim 66\%$ after 60 min of UV-LED irradiation at 280 nm. This may be ascribed to the maximum absorption wavelength of CIP at 275 nm (Fig. S3). The apparent rate constant for the 280 nm UV-LED treatment reached 0.0181 min^{-1} , with a half-time of 38.3 min. To the best of our knowledge, there has been no relevant research using different wavelengths of UV irradiation, except at 254 nm, for CIP degradation. In the previous study [14], low rate constants were observed for the direct degradation of CIP by a 254 nm mercury lamp, but no data regarding other wavelengths was reported.

The results of the UV/ H_2O_2 degradation experiments using UV-LEDs of different wavelength are presented in Fig. 2b. Obviously, treatment using 280 nm UV-LED/ H_2O_2 was the most effective, followed by 310 and 365 nm. The removal efficiencies at 280, 310 and 365 nm UV-LED/ H_2O_2 reached $\sim 99\%$, $\sim 97\%$ and $\sim 73\%$, respectively, within 60 min. As shown in Table 2, the apparent rate constants in the UV-LED/ H_2O_2 system increased from 0.0067 min^{-1} at 255 nm to 0.0759 min^{-1} at 280 nm, and then decreased to 0.0191 min^{-1} at 365 nm. The half-time of CIP in the 280 nm/ H_2O_2 system was

Table 1
Operational parameters of tandem mass spectrometry.

Parameter (unit)	TripleTOF 5600+	TripleQuad 5500
Ion source mode	Positive	Positive
Scan mode	Full scan	MRM*
ESI needle voltage (V)	3500	3500
Turbo-gas temperature ($^{\circ}\text{C}$)	350	350
Curtain gas pressure (psi)	40	40
Nebulizer gas pressure (psi)	35	35
Auxiliary gas pressure (psi)	40	40
Declustering potential (V)	60	60
CID energy (eV)	20 ± 15	–

* MRM: multi reaction monitoring.

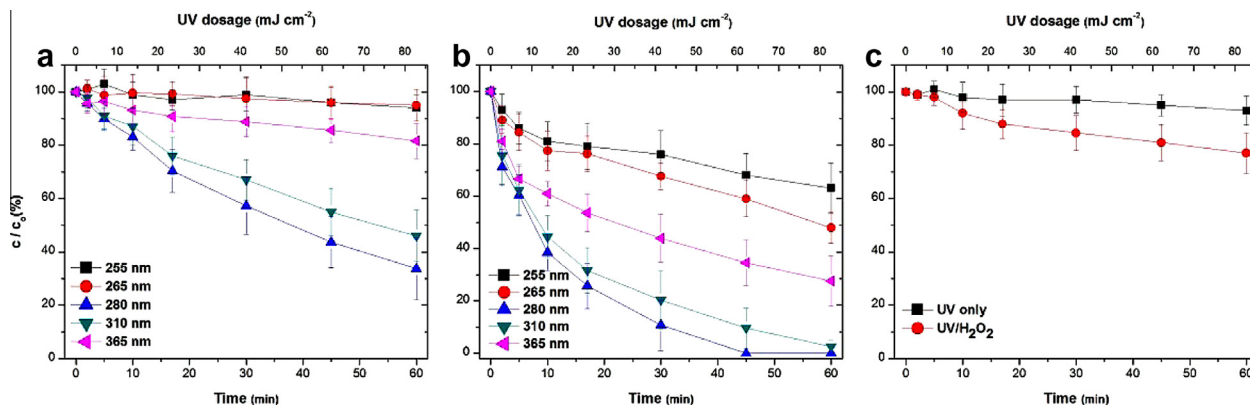


Fig. 2. Removal efficiency of ciprofloxacin. (a) UV only, (b) UV/H₂O₂, (c) TOC. Experimental conditions: solution temperature 25 ± 2 °C, pH 6.5–7.2, [ciprofloxacin]₀ = 30 μM, [H₂O₂]₀ = 300 μM (only in UV/H₂O₂ experiment). The removal efficiencies of different wavelengths have been calculated based on irradiating dosages. All the experiments were carried out in triplicate with error bars representing the standard error of the mean.

Table 2
Apparent rate constants and half-lives of CIP in various wavelength UV-LEDs treatment.

Reaction	Confidence coefficient	Rate constant (min ⁻¹)	Half-time (min)
255 nm only	0.8658	0.0003	2310.5
265 nm only	0.9952	0.0019	770.1
280 nm only	0.9988	0.0181	38.3
310 nm only	0.9953	0.0129	53.7
365 nm only	0.9541	0.0030	231.1
255 nm/H ₂ O ₂	0.9125	0.0067	103.4
265 nm/H ₂ O ₂	0.9939	0.0106	65.4
280 nm/H ₂ O ₂	0.9958	0.0759	9.1
310 nm/H ₂ O ₂	0.9909	0.0549	12.6
365 nm/H ₂ O ₂	0.9388	0.0191	36.5

9.1 min, suggesting that CIP can undergo fast degradation. Compared with the results of the UV-LED-only experiments, the degradation effectiveness of UV-LED/H₂O₂ increased at the same wavelength, which may be ascribed to the promotion of OH[•] oxidation.

The variation of TOC is presented in Fig. 2c. For a 10 mg L⁻¹ (30 μM) CIP solution, the apparent TOC value was 5.972 ± 0.346 mg L⁻¹ at time zero. After a reaction time of 60 min, only 7% and 23% TOC were removed in the 280 nm UV-LED-only and the UV-LED/H₂O₂ system, respectively. These low mineralization efficiencies can be attributed to two factors: (1) a lack of H₂O₂ and (2) the low irradiation intensity (fluence rate) of the UV-LED chips. First, the [H₂O₂]:[CIP] was 10:1 in the current study, which was lower than the basic stoichiometric molar ratio for total degradation ([H₂O₂]:[CIP] = 47:1), resulting in an incomplete degradation of CIP. Second, the photo-quantum yield in a UV-based reaction is related to the irradiation intensity of light source; thus, the low irradiation intensity (0.023 mW cm⁻²) of UV-LED resulted in a low generating efficiency of hydroxyl free radicals. This may also contribute to the low mineralization efficiency. In the research that used high-intensity irradiation treatment at 254 nm (up to 0.43 mW cm⁻²), the mineralization efficiency was significantly higher (>60%) [25].

3.2. MS² analysis of CIP

According to the apparent mass-to-charge ratio equation (Eq. (2)), [CIP+H]⁺ had a *m/z* of 332.1405. An extract ion chromatogram of *m/z* = 332.1405 was obtained from the HRMS data, and thirty-seven distinct fragments were observed (Fig. S4). To avoid redundancy, the top 10 fragments in term of intensity were selected (Table 3). Nine compositions (included [CIP+H]⁺) were directly assigned to these fragments.

$$\frac{m}{z} = \frac{M + nH}{n} \quad (2)$$

where *m* is the apparent mass of the targeted molecular ion, *z* is the electric charge of targeted molecular ion, *m/z* represents the apparent mass-to-charge ratio, *M* is the exact mass of the targeted molecule, *n* is the number of electric charge, and *H* represents the exact mass of a proton.

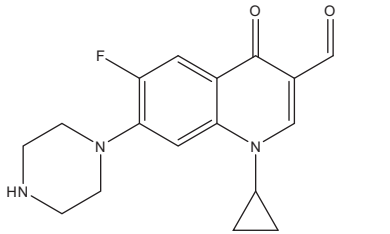
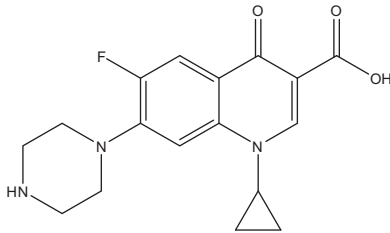
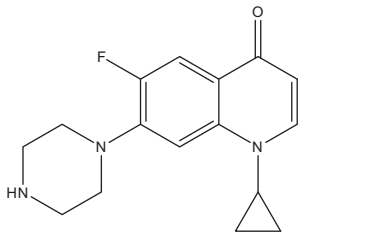
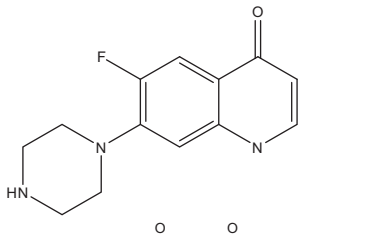
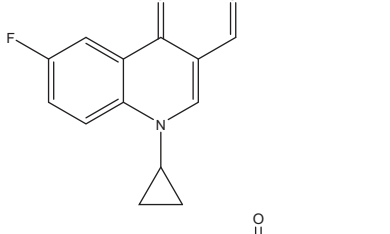
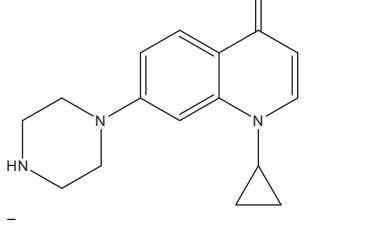
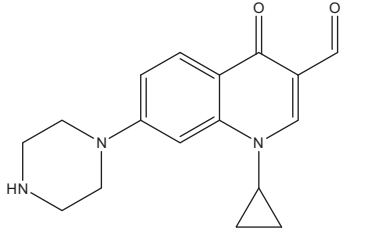
The molecular structure of CIP is presented in Fig. S5. The central functional group is a quinolone moiety, and the peripheral moieties include a carboxyl group, a cyclopropyl group, a piperazine ring and fluorine. CID can induce cleavages of these moieties, and their losses may be single or multiple, resulting in different characteristic fragments. The fragment with an observed *m/z* = 314.1298 had the highest intensity (set as 100%) and was assigned as [C₁₇H₁₇FN₃O₂]⁺, which had an approximate 18 Da (H₂O) difference compared to [CIP+H]⁺. The fragment with the third highest intensity (69.2%) was [C₁₆H₁₉FN₃O]⁺ (*m/z* = 288.1497), which had an approximate 44 Da (CO₂) difference compared to [CIP+H]⁺. These two fragments were also observed in the previous literature [26], and they reflected the existence of the terminal carboxyl group. Their high intensities suggested that the neutral losses of CO₂ and H₂O were the dominant cleavages of CIP under the current HRMS conditions.

The fragment *m/z* = 245.1079 was assigned as [C₁₃H₁₂FN₃O]⁺, and it may be the residual moiety that had previously lost both the carboxyl (MW 43.9892 Da) and the cyclopropyl (MW 43.0548 Da) groups. The fragment *m/z* = 231.0576 ([C₁₃H₁₀FN₃O₂]⁺) may be formed through loss of the piperazine ring (C₄H₇N₂, MW 83.0609 Da) and the hydroxyl (MW 18.0100 Da). Furthermore, the fragment *m/z* = 294.1237 ([C₁₇H₁₆N₃O₂]⁺) may evolve from the cleavage of the C–F bond and the hydroxyl, while the fragment *m/z* = 268.1447 ([C₁₆H₁₈N₃O]⁺) may evolve from the cleavage of the C–F bond and the carboxyl. Of note, the fragment *m/z* = 205.0773 ([C₁₁H₁₀FN₂O]⁺) may include a cleavage at the cyclohexene in the quinolone moiety. The last fragment, *m/z* = 204.0156 ([C₁₀H₉FN₃O]⁺), was generated by the loss of the piperazine ring and the cyclopropyl group. These characteristic fragments can provide useful information for subsequent interpretation of the intermediates.

3.3. Structure elucidation of intermediates in UV-LED-only experiment

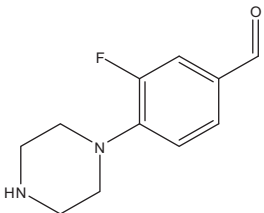
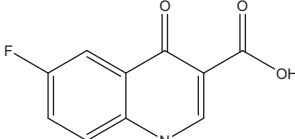
According to the published studies, four sites in CIP, including the C–F bond, the C=C bond in the quinolone moiety, the piperazine ring and the cyclopropyl, may be attacked in the UV system and UV/H₂O₂ system [25]. The computed results of the molecular

Table 3
MS/MS ions observed in the spectrum of [CIP+H]⁺.

<i>m/z</i>		Intensity (%)	Error (Da)	Assigned molecular formula	MW difference with [CIP+H] ⁺	Molecular structure	Characteristic moiety
Observed	Calculated						
314.1298	314.1305	100	0.001	[C ₁₇ H ₁₇ FN ₃ O ₂] ⁺ ([CIP+H–H ₂ O] ⁺)	18.0104		Hydroxyl
332.1405	332.1410	77.4	0.001	[CIP+H] ⁺ C ₁₇ H ₁₈ FN ₃ O ₃	0		–
288.1497	288.1512	69.2	0.001	[C ₁₆ H ₁₉ FN ₃ O] ⁺ ([CIP+H–CO ₂] ⁺)	43.9905		Carboxyl
245.1079	245.0964	35.9	0.011	[C ₁₃ H ₁₂ FN ₃ O] ⁺ ([CIP+H–CO ₂ –C ₃ H ₇] ⁺)	87.0323		Carboxyl, cyclopropyl
231.0576	231.0695	24.3	0.012	[C ₁₃ H ₁₀ FN ₂ O] ⁺ ([CIP+H–H ₂ O–C ₄ H ₇ N ₂] ⁺)	101.0826		Hydroxyl, piperazine
268.1447	268.1450	13.1	0.000	[C ₁₆ H ₁₈ N ₃ O] ⁺ ([CIP+H–CO ₂ –HF] ⁺)	63.9955		Fluorine, carboxyl
314.8798	–	9.8	–	–	17.2604	–	–
294.1237	294.1242	7.9	0.000	[C ₁₇ H ₁₆ N ₃ O ₂] ⁺ ([CIP+H–H ₂ O–HF] ⁺)	38.0165		Fluorine, hydroxyl

(continued on next page)

Table 3 (continued)

m/z		Intensity (%)	Error (Da)	Assigned molecular formula	MW difference with [CIP+H] ⁺	Molecular structure	Characteristic moiety
Observed	Calculated						
205.0773	205.0777	5.3	0.000	[C ₁₁ H ₁₀ FN ₂ O] ⁺ ([CIP+H–C ₆ H ₉ NO ₂) ⁺)	127.0629		Quinolone
204.0156	204.0097	5.3	0.001	[C ₁₀ H ₅ FNO ₃] ⁺ ([CIP +H–C ₃ H ₇ –C ₄ H ₇ N ₂) ⁺)	128.1246		Piperazine, cyclopropyl

properties (Fig. S6 and Table S2) were also in agreement with these previous studies and Scheme 2. Due to their low bond energies, the cleavage occurred in the N(11)–C(12) and C(1)–F(8) bonds more easily than in other C–C, N–C and C–O bonds. Among all of the C–C bonds, the one linking C(20) and C(21) in the cyclopropyl group had the lowest energy and was the easiest to break. The screening of potential intermediates from the HRMS data was based on the possible transformations of these sites. Eventually, three intermediates were confirmed in the 280 nm UV-LED-only experiment. They were identified as C₁₅H₁₆FN₃O₃ (m/z 306.1), C₁₇H₁₉N₃O₄ (m/z 330.1) and C₁₇H₁₈FN₃O₄ (m/z 348.1) (Table 4 and Scheme 1). The observed fragments of CIP and its intermediates are summarized in Table S3.

Intermediate C₁₅H₁₆FN₃O₃ (A) had a MW of 305.1176 Da, which was sustained by a 26.0156 Da difference with that of intact CIP. As reported by other studies [27], intermediate A was desethylene CIP, which may be formed through the cleavage of C₂H₂ (MW 26.0156 Da) at the piperazinyl moiety. The MS² spectrum showed that the primary fragments were m/z 288.1155, 268.1089, 218.0487 and 190.0538 (Fig. S7). The observation of this intermediate implied that UV-LED irradiation induced the direct destruction of the piperazine ring.

Intermediate C₁₇H₁₉N₃O₄ (B) had a MW of 329.1376 Da. This intermediate had a 1.9956 Da difference from CIP, which implied that its transformation involved the substitution of some peripheral moiety. The fragments of intermediate B included m/z 312.1351, 286.1553, 243.1127, 229.0602, and so on (Fig. S8), which had formation patterns similar to the m/z 314.1298, 288.1497, 245.1079 and 231.0576 fragments, respectively, in the CIP MS² spectrum (Table S3), indicating the presences of carboxyl, cyclopropyl, and piperazinyl groups. In the CIP MS² spectrum (Fig. S8), the fragments m/z 268.1447 and 294.1237 both represented the C–F bond. However, the corresponding characteristic fragments were absent in the MS² spectrum of intermediate B, suggesting that it may have lost the C–F bond. Therefore, the transformation from CIP to intermediate B may involve the elimination of a fluorine atom (MW 18.9984 Da) and the addition of a hydroxyl (MW 17.0027 Da) (Scheme 1). In the previous study using UV irradiation at 254 nm, an intermediate with a similar structure was also observed [14]. These results suggested that direct 280 nm UV-LED irradiation attacked the C–F bond, followed by the addition of a hydroxyl group on the quinolone.

Intermediate C₁₇H₁₈FN₃O₄ (C) had a MW of 347.1281 Da. This intermediate had a 15.9951 Da difference from CIP, suggesting the addition of an oxygen atom or the substitution of a hydrogen

atom by a hydroxyl. The primary fragments had m/z 330.1235, 304.1443, and 261.1003 (Fig. S9), indicating the presence of both carboxyl and cyclopropyl groups (Table S3). Furthermore, the minor fragments m/z 247.0517 and m/z 310.1182 implied the existences of the piperazinyl ring and fluorine. These results suggested that the 15.9951 Da transformation may be located at the quinolone moiety. Therefore, intermediate C may have a hydroxyl substitution at Site 10 of CIP [28].

The relative intensity variations and abundance variations of these intermediates are presented in Fig. 3. The intensity of intermediate B increased to approximate 2.0×10^5 at 50 min and then showed a decreasing tendency. Intermediate A increased to 1.0×10^5 at 17 min and disappeared at 40 min. The variation tendency of intermediate C was relative inconsistent with a maximal intensity of 3.2×10^4 at 10 min. Although the exact concentrations of these intermediates were not determined accurately, as we did not have authentic standards for them, these data are still important in evaluating the variation tendency and abundance of these intermediates. These results suggested that UV-LED irradiation mainly induced transformations of the peripheral moieties. Undoubtedly, the hydroxyl substitution of C–F bond at Site 5 was the dominant transformation in terms of the relative intensity under irradiation at 280 nm UV-LED. Of note, intermediate B was also observed in the reported study using a low-pressure mercury lamp with UV irradiation at 254 nm [14].

3.4. Elucidation of the structure of preliminary intermediates in UV-LED/H₂O₂ treatment

The addition of H₂O₂ may induce a more complicated degradation of CIP, which may be ascribed to the nonselective oxidation of OH[•]. However, identification of all these intermediates would be time-consuming and somewhat inadvisable. Therefore, a compact two-step procedure was used for the identification of the intermediates in the UV-LED/H₂O₂ treatment. The first step aimed at discovering the preliminary intermediates, that is, those generated by a one-step transformation from CIP, and the second step focused on seeking the further-transformed intermediates. In the first step, six intermediates were identified from the HRMS data. Among these intermediates, three were also observed in the UV-LED-only experiment, including intermediates A, B and C. However, other three intermediates, C₁₆H₁₈FN₃O₂ (m/z 304.1), C₁₅H₁₄FN₃O₅ (m/z 336.1) and C₁₇H₁₆FN₃O₄ (m/z 346.1), were observed only in the UV-LED/H₂O₂ experiment (Scheme 2).

Table 4
Structure elucidation of stable intermediates.

No.	Name	Molecular formula	Nominal mass (Da)	Calculated mass (Da) ^a	Mass error range ($\times 10^{-3}$ Da) ^b	Average isotope ratio difference (%) ^c	MaS (%) ^d	Observed reaction ^e
	CIP	C ₁₇ H ₁₈ FN ₃ O ₃	331.1332	332.1405	2.8–4.6	3.1	97.2	–
1	A	C ₁₅ H ₁₆ FN ₃ O ₃	305.1176	306.1248	–0.5–2.3	5.6	96.3	UV-LED-only and UV/H ₂ O ₂
2	B	C ₁₇ H ₁₉ N ₃ O ₄	329.1376	330.1448	–0.8–1	4.7	96.3	UV-LED-only and UV/H ₂ O ₂
3	C	C ₁₇ H ₁₈ FN ₃ O ₄	347.1281	348.1354	1.6–3.7	2.8	81.1A	UV-LED-only and UV/H ₂ O ₂
4	D	C ₁₆ H ₁₈ FN ₃ O ₂	303.1383	304.1456	–0.9–1.2	3.6	88.1A	UV/H ₂ O ₂
5	E	C ₁₅ H ₁₄ FN ₃ O ₅	335.0918	336.0990	0.2–2.6	2.7	67.8A	UV/H ₂ O ₂
6	F	C ₁₇ H ₁₆ FN ₃ O ₄	345.1125	346.1198	0.6–0.9	5.1	94.3A	UV/H ₂ O ₂
7	G	C ₁₇ H ₁₈ FN ₃ O ₅	363.1230	364.1310	–1.7–3.6	4.3	96.1	UV/H ₂ O ₂
8	H	C ₁₅ H ₁₈ FN ₃ O ₃	307.1332	308.1405	–1.2–2.3	3.6	87.6	UV/H ₂ O ₂

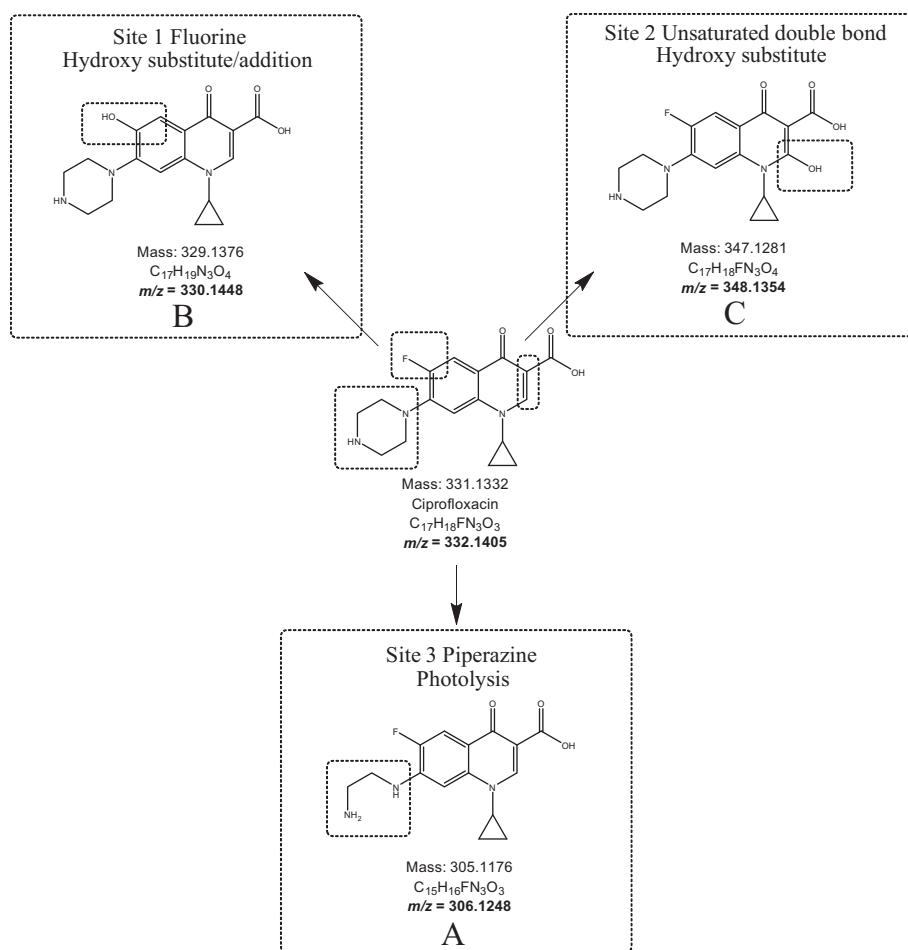
^a Calculated theoretical mass of pseudomolecular ion [M+H]⁺ of intermediates.

^b Difference between measured and calculated theoretical mass.

^c Difference between measured and calculated isotope distribution.

^d MaS represents the Matching Score, which indicates the percentage of intensity in regard to MS/MS fragments which can be directly matched with given .mol file (intermediate screening procedure can be seen in [Supporting Information](#)).

^e Intermediates observed in UV and/or UV/H₂O₂ reactions.



Scheme 1. Proposed generative pathways for the CIP intermediates under 280 nm UV-LED irradiation.

Intermediate C₁₆H₁₈FN₃O₂ (D) had a MW of 303.1383 Da. This intermediate had a 27.9945 Da difference from CIP, and its primary fragments included *m/z* of 221.0722, 261.1036, 284.1396 and 220.0653 (Fig. S10). In the absence of any carboxyl characteristic fragment (Table S3), it can be concluded that the formation of intermediate D involved the substitution of the terminal carboxyl (–44 Da) by a hydroxyl (+18 Da). The observation of this intermediate inferred that OH[•] can attack the terminal carboxyl of CIP.

Intermediate C₁₅H₁₄FN₃O₅ (E) had a MW of 335.0917 Da, which represented a 3.9588 Da difference with that of CIP. The MS² spectrum showed that the primary fragments were *m/z* 316.0928, 298.0820, 275.0541 and 270.0895 (Fig. S11). The fragment *m/z* 316.0928 ([C₁₅H₁₄N₃O₅]⁺) implied the presence of a C–F bond, and the *m/z* 298.0820 ([C₁₅H₁₂N₃O₄]⁺) indicated the presences of both a C–F bond and a hydroxyl. Therefore, it was concluded that the transformation site may be located at the cyclopropyl group or

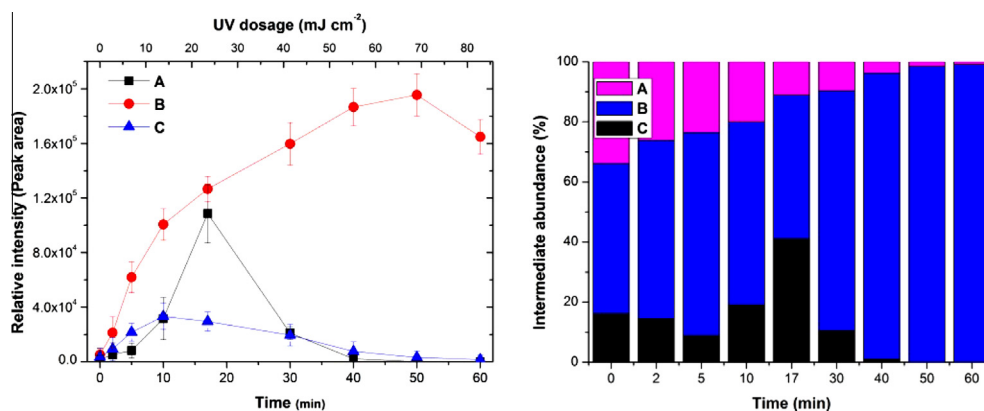
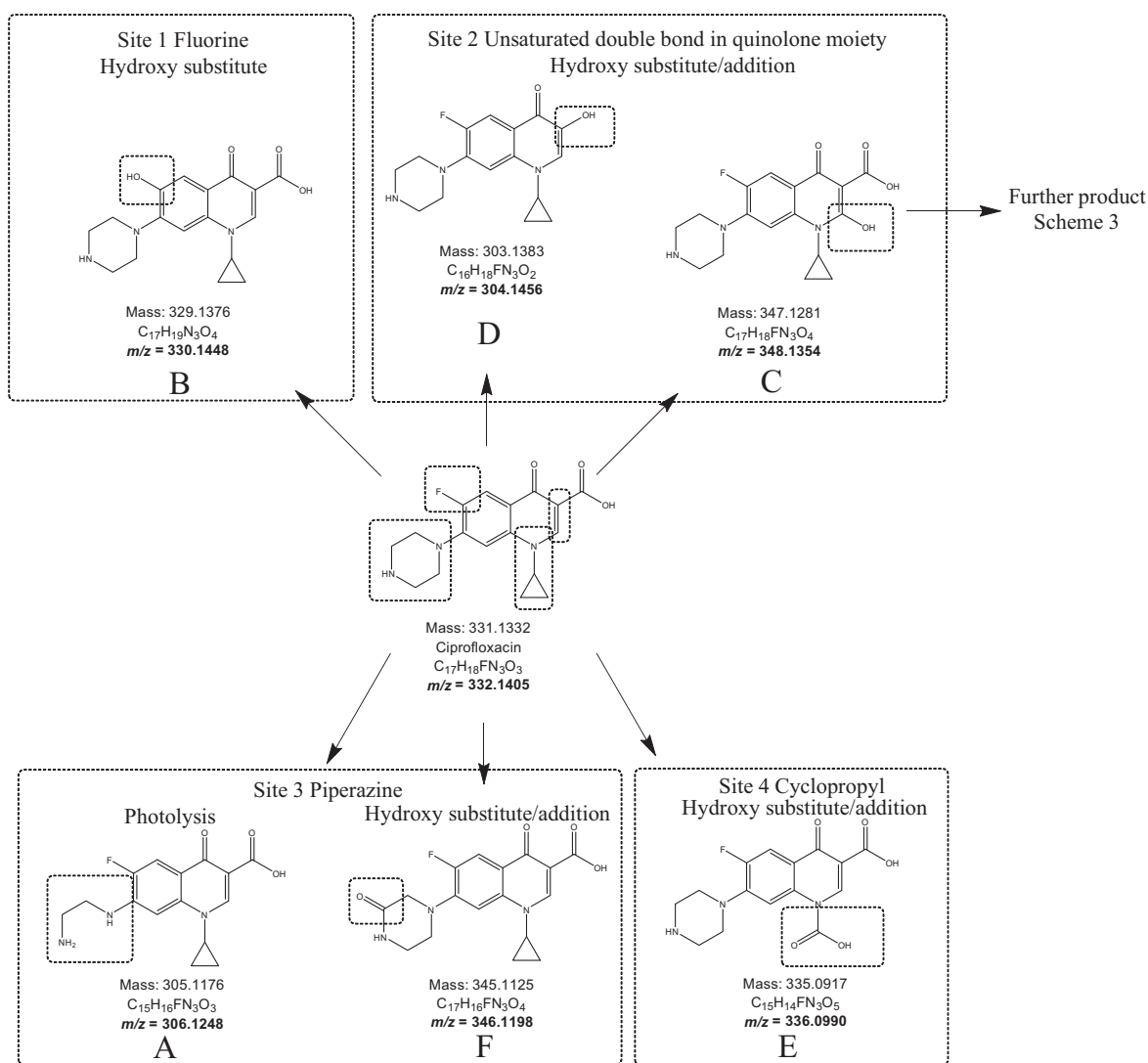


Fig. 3. Relative intensity and abundance variations of CIP intermediates in 280 nm UV only experiment. The relative intensity indicates the peak area of extract ion chromatogram from MS/MS data, which has a dimensionless unit.



Scheme 2. Proposed generative pathways for the CIP intermediates under 280 nm UV-LED/H₂O₂ treatment.

the piperazine ring. According to the previous study [27], this intermediate was formed by the oxidation of the cyclopropyl group.

Intermediate C₁₇H₁₆FN₃O₄ (F) had a MW of 345.1125 Da. Its CID fragments included m/z 328.1097, 287.0708, 302.1305, 259.0762

(Fig. S12). The fragments m/z 328.1097 and m/z 302.1305 represented the existence of a terminal carboxyl, and m/z 259.0762 showed the cyclopropyl group to be a characteristic fragment. The absence of piperazinyll and fluorine characteristic fragments inferred that the transformation may occur in these two sites.

Eventually, intermediate F was identified to have a substitution of two hydrogen atoms in piperazinyl by an oxygen atom, forming a ketone.

Fig. 4 presents the relative intensity and abundance variations of these six intermediates. Intermediate C had the highest intensity ($\sim 1.4 \times 10^6$ at 10 min), indicating that it may be the dominant product. The observation of these six intermediates implied that all of the peripheral moieties and the quinolone moiety were susceptible to OH. These results were in agreement with those reported in the previous study [25]. However, in the previous study using visible light photocatalysis, the cleavage of the piperazine ring (forming intermediate A) was identified as the dominant transformation mechanism [29]. This difference may be ascribed to the difference in reaction conditions, such as the light sources and the application of catalysts.

3.5. Destruction on the quinolone moiety

Intermediate C was the dominant among the six observed preliminary intermediates. Therefore, the second-step search focused on further products derived from it. After screening, only two further intermediates were identified, including $C_{15}H_{18}FN_3O_3$ (H, m/z 308.1, Fig. S13) and $C_{17}H_{18}FN_3O_5$ (G, m/z 364.1, Fig. S14). Other possible further intermediates may be generated in the degradation process; however, no evidence of these intermediates was observed in the current study.

A consecutive oxidation pathway was proposed (Scheme 3), which included a hydroxyl addition on the C=C (forming intermediate C), cleavage of this C=C and then double oxidation to a ketone (intermediate G), and cleavage and oxidation of the carboxyl (hypothetical product $C_{16}H_{18}FN_3O_4$), ultimately forming intermediate H. Intermediates C, G and H were observed and determined, which provided convincing evidence for this hypothesis.

Fig. 5 presents the relative intensity and abundance variations of these intermediates. The relative intensity of intermediate C rapidly increased to $\sim 1.4 \times 10^6$ at 10 min and then slowly decreased to $\sim 0.4 \times 10^6$ within 60 min. The relative intensity of intermediate G increased during the initial 45 min and then slowly decreased. Of note, intermediate H continuously increased for the entire 60 min. These results suggested a generating sequence of intermediates C, G and H, in accordance with the proposed consecutive oxidation pathway. It also implied that UV-LED/ H_2O_2 treatment at 280 nm can destroy the core quinolone structure of CIP.

3.6. Antibacterial activity

To estimate the residual antibacterial activity of a treated CIP solution, a microbial analysis was performed by using *E. coli* as the reference organism. The variation of antibacterial activity was determined by measuring the inhibition halo formed around the micro-drop seeded on the agar plate. Fig. 6 presents the typical results, where the inhibition halo of the UV-LED-only samples slightly decreased as the irradiation time increased. In contrast, the inhibition halo diameter of the UV/ H_2O_2 samples decreased from 27.5 mm (control) to 12.5 mm (30 min), and finally it disappeared after a 45-min reaction, indicating a significant decline in antibacterial activity. The mineralization ratios of these reactions were low; therefore, it can be concluded that the variation of antibacterial activity can be mainly attributed to the modifications of the CIP functional moieties.

CIP is now known to interact with two related but distinct targets, DNA gyrase and topoisomerase IV, inducing further DNA replication failure in bacteria cells. The quinolone moiety is the basic framework of CIP, while the peripheral moieties play additional important roles in antibacterial activity. The carboxyl and carbonyl groups are critical for cleaving or perturbing DNA and

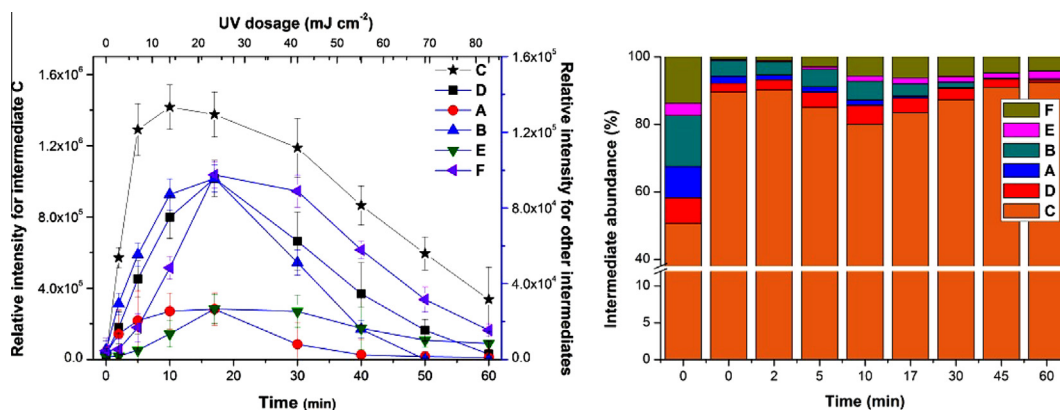
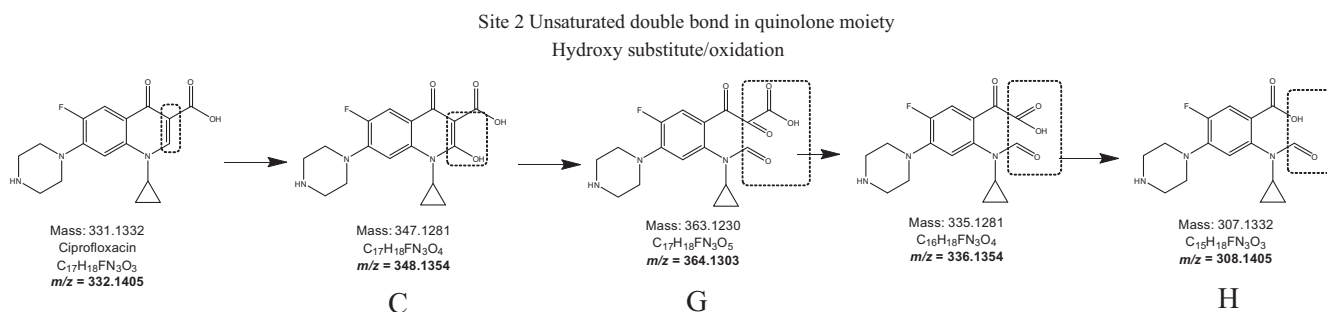


Fig. 4. Relative intensity and abundance variations of preliminary intermediates in 280 nm UV/ H_2O_2 experiment. The relative intensity indicates the peak area of extract ion chromatogram from MS/MS data, which has a dimensionless unit.



Scheme 3. Consecutive oxidation pathway of unsaturated double bond on quinolone moiety and the possible oxidized intermediates under 280 nm UV-LED/ H_2O_2 treatment.

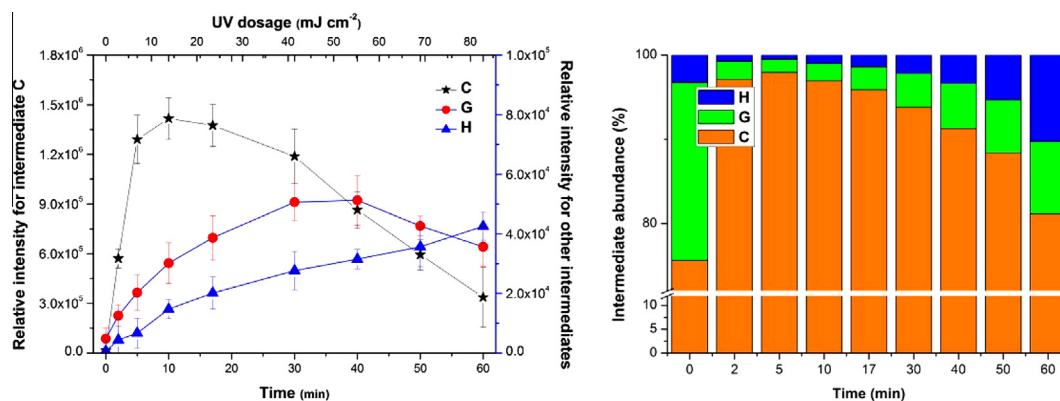


Fig. 5. Relative intensity and abundance variations of further intermediates in 280 nm UV/H₂O₂ experiment. The relative intensity indicates the peak area of extract ion chromatogram from MS/MS data, which has a dimensionless unit.

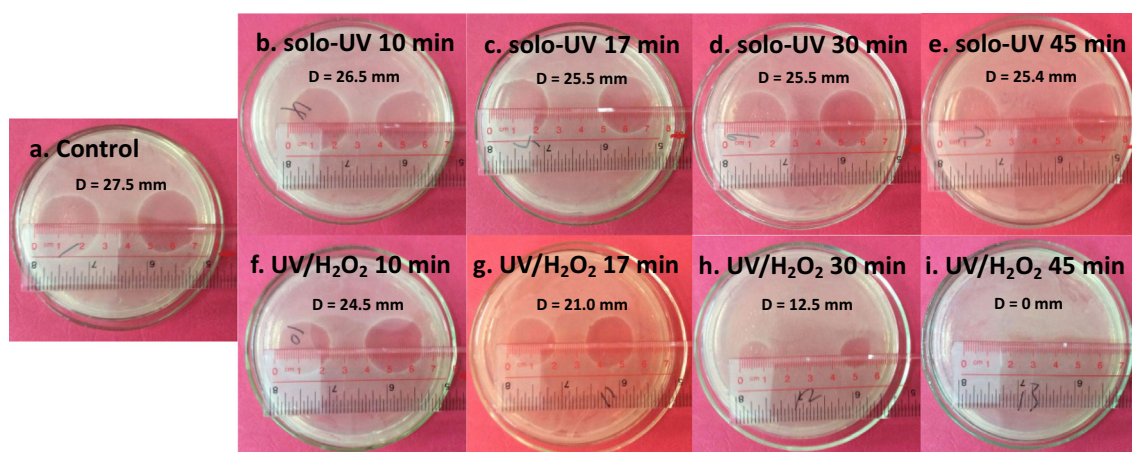


Fig. 6. *Escherichia coli* inhibition halo at different times of 280 nm solo-UV-LED irradiation and UV-LED/H₂O₂ reaction.

are essential for reducing bacteria resistance [30]. The piperazine ring can directly interact with DNA gyrase or topoisomerase IV [31]. The cyclopropyl is part of the enzyme–DNA binding complex and has a hydrophobic interaction with the major groove of DNA [32]. Furthermore, the fluorine at Site 5 can improve the antibacterial activity of CIP. Theoretically, transformations of the carboxyl (intermediate D), the piperazine ring (intermediates A and F), the cyclopropyl (intermediate E) and the C–F bond (intermediate B) all weaken the antibacterial activity of CIP. Of note, because Site 10 at CIP is very close to the site for DNA gyrase (or topoisomerase IV) binding, the addition of a hydroxyl on this site (intermediate C) may also inhibit the antibacterial activity [33].

In the UV-LED-only reaction, intermediate B was the dominant product in regard to the relative intensity (Fig. 3); therefore, the slight reduction of antibacterial activity is mostly ascribed to the formation of intermediate B. Because the C–F bond at Site 5 is not a critical functional group, its elimination had a limited effect on antibacterial activity (Fig. 6e). In contrast, the modifications of all of the CIP functional groups were observed in the UV/H₂O₂ reaction (Schemes 2 and 3). Intermediate C was the primary product with the highest intensity, and the consecutive oxidation of it to form intermediate H resulted in critical damage to the quinolone moiety, which should show significant inhibition of antibacterial activity. This inhibition was confirmed by the rapid decline of the inhibition halo diameter (Fig. 6i). Of note, there was still 81% of the TOC left after the 45-min UV/H₂O₂ reaction (Fig. 2c), suggesting that the incomplete degradation of CIP can still induce a significant reduction of antibacterial activity.

3.7. EE/O calculation of UV-LED/H₂O₂ systems

The results of the UV-LED/H₂O₂ treatment in terms of the removal efficiency and antibacterial activity reduction above were observed to be rather good. However, it is necessary to evaluate its cost. The electrical energy per order (EE/O) values were calculated for the 280 nm UV-LED and UV-LED/H₂O₂ systems. Detailed information about the calculation method was reported in Ref. [34]. The EE/O value was calculated by taking into account both the electrical energy and chemical oxidant needed in devices [35]. The calculation results are shown in Table S4. The EE/O_e values were calculated to be 0.0115 and 0.0027 kWh/m³/order, respectively, for the 280 nm UV-LED only treatment and UV-LED/H₂O₂ treatment. The EE/O value for chemical energy considering the chemical cost was calculated to be 0.0064 kWh/m³/order for the 280 nm UV-LED/H₂O₂ treatment. The EE/O values obtained were significantly lower than the values in experiments using conventional mercury lamps [36].

4. Conclusions

To conclude, different wavelength (255–365 nm) UV-LED/H₂O₂ treatments were able to degrade CIP. The UV-LED/H₂O₂ treatment at 280 nm had the highest degradation effectiveness. Three intermediates were identified in the UV-LED-only experiment, and their transformations involved the substitution of the C–F bond by a hydroxyl (intermediate B), the addition of a hydroxyl on cyclohex-

ene (intermediate C) and the breakage of the piperazine ring (intermediate A). In the UV-LED/H₂O₂ experiment, eight intermediates were elucidated, and the transformation involved the oxidation of carboxyl (intermediate D), cyclopropyl (intermediate E) and piperazine (intermediate F). Furthermore, a consecutive oxidation pathway, following the order of CIP and intermediates C, G, E and H, was proposed. Microbial analysis proved that this consecutive destruction of quinolone can reduce the antibacterial activity of CIP. Because quinolone antibiotics all have a similar quinolone moiety, our results implied that 280 nm UV-LED/H₂O₂ can be used as an effective method to degrade quinolones and reduce their antibacterial activity.

Acknowledgments

This project was supported by the National Natural Science Foundation of China (Grant No. 51308224), the Science and Technology Planning Project of Guangdong Province, China (Grant No. 2014A020216014), and the State Key Program of the National Natural Science Foundation of China (Grant No. 21037001).

Appendix A. Supplementary data

Supplementary data associated with this article can be found, in the online version, at <http://dx.doi.org/10.1016/j.cej.2016.01.006>.

References

- [1] Z. Qinjin, J. Ai, W. Yi, L. Hong, W. Kunping, P. Hui, D. Zhaomin, H. Jianying, Occurrences of three classes of antibiotics in a natural river basin: association with antibiotic-resistant *Escherichia coli*, *Environ. Sci. Technol.* 48 (2014) 14317–14325.
- [2] T.M. Lapara, T.R. Burch, P.J. McNamara, D.T. Tan, Y. Mi, J.J. Eichmiller, Tertiary-treated municipal wastewater is a significant point source of antibiotic resistance genes into Duluth-Superior Harbor, *Environ. Sci. Technol.* 45 (2011) 9543–9549.
- [3] K. Oberlé, M.J. Capdeville, T. Berthe, H. Budzinski, F. Petit, Evidence for a complex relationship between antibiotics and antibiotic-resistant *Escherichia coli*: from medical center patients to a receiving environment, *Environ. Sci. Technol.* 46 (2012) 1859–1868.
- [4] A. Ludmilla, M. Anastasios, S. Garrison, Inhibition of photosynthesis by a fluoroquinolone antibiotic, *Environ. Sci. Technol.* 44 (2010) 1444–1450.
- [5] L. Min, D. Wei, H. Zhao, Y. Du, Genotoxicity of quinolones: substituents contribution and transformation products QSAR evaluation using 2D and 3D models, *Chemosphere* 95 (2014) 220–226.
- [6] Y. Pi, J. Feng, M. Song, J. Sun, Degradation potential of ofloxacin and its resulting transformation products during Fenton oxidation process, *Chin. Sci. Bull.* 59 (2014) 2618–2624.
- [7] C. Liu, V. Nanaboina, G.V. Korshin, W. Jiang, Spectroscopic study of degradation products of ciprofloxacin, norfloxacin and lomefloxacin formed in ozonated wastewater, *Water Res.* 46 (2012) 5235–5246.
- [8] M. Mahdi-Ahmed, S. Chiron, Ciprofloxacin oxidation by UV-C activated peroxymonosulfate in wastewater, *J. Hazard. Mater.* 265 (2014) 41–46.
- [9] X.V. Doorslaer, K. Demeestere, P.M. Heynderickx, M. Caussyn, H.V. Langenhove, F. Devlieghere, V. An, J. Dewulf, Heterogeneous photocatalysis of moxifloxacin: identification of degradation products and determination of residual antibacterial activity, *Appl. Catal. B* 138 (2013) 333–341.
- [10] L.V. Santos, A.M. Meireles, L.C. Lange, Degradation of antibiotics norfloxacin by Fenton, UV and UV/H₂O₂, *J. Environ. Manage.* 154 (2015) 8–12.
- [11] X.V. Doorslaer, K. Demeestere, P.M. Heynderickx, H.V. Langenhove, J. Dewulf, UV-A and UV-C induced photolytic and photocatalytic degradation of aqueous ciprofloxacin and moxifloxacin: reaction kinetics and role of adsorption, *Appl. Catal. B* 101 (2011) 540–547.
- [12] J. Di, J. Xia, Y. Ge, H. Li, H. Ji, H. Xu, Q. Zhang, H. Li, M. Li, Novel visible-light-driven CQDs/Bi₂WO₆ hybrid materials with enhanced photocatalytic activity toward organic pollutants degradation and mechanism insight, *Appl. Catal. B* 168 (2015) 51–61.
- [13] P. Huo, Z. Lu, X. Liu, D. Wu, X. Liu, J. Pan, X. Gao, W. Guo, H. Li, Y. Yan, Preparation photocatalyst of selected photodegradation antibiotics by molecular imprinting technology onto TiO₂/fly-ash cenospheres, *Chem. Eng. J.* 189–190 (2012) 75–83.
- [14] H.G. Guo, N.Y. Gao, W.H. Chu, L. Li, Y.J. Zhang, J.S. Gu, Y.L. Gu, Photochemical degradation of ciprofloxacin in UV and UV/H₂O₂ process: kinetics, parameters, and products, *Environ. Sci. Pollut. Res.* 20 (2013) 3202–3213.
- [15] S. Babić, M. Perišaa, I. Škorićb, Photolytic degradation of norfloxacin, enrofloxacin and ciprofloxacin in various aqueous media, *Chemosphere* 91 (2013) 1635–1642.
- [16] S. Vilhunen, M. Sillanpää, Recent developments in photochemical and chemical AOPs in water treatment: a mini-review, *Rev. Environ. Sci. Bio/Technol.* 9 (2010) 323–330.
- [17] W.K. Jo, R.J. Tayade, New generation energy-efficient light source for photocatalysis: LEDs for environmental applications, *Ind. Eng. Chem. Res.* 53 (2014) 2073–2084.
- [18] S.H. Vilhunen, M.E. Sillanp, Ultraviolet light emitting diodes and hydrogen peroxide in the photodegradation of aqueous phenol, *J. Hazard. Mater.* 161 (2009) 1530–1534.
- [19] A. Jamali, R. Vanraes, P. Hanselaer, T.V. Gerven, A batch LED reactor for the photocatalytic degradation of phenol, *Chem. Eng. Process.* 71 (2013) 43–50.
- [20] C.S. Chiou, C.T. Chang, C.C. Chang, C.Y. Chang, Photodegradation kinetics of formaldehyde using light sources of UVA, composed silver titanium oxide photocatalyst, *J. Hazard. Mater.* 155 (2008) 164–172.
- [21] R.J. Tayade, T.S. Natarajan, H.C. Bajaj, Photocatalytic degradation of methylene blue dye using ultraviolet light emitting diodes, *Ind. Eng. Chem. Res.* 48 (2009) 10262–10267.
- [22] E. Repo, S. Rengaraj, S. Pulkka, E. Castangnoli, S. Suihkonen, M. Sapanen, M. Sillanpää, Photocatalytic degradation of dyes by CdS microspheres under near UV and blue LED radiation, *Sep. Purif. Technol.* 120 (2013) 206–214.
- [23] M. Izadifard, G. Achari, C.H. Langford, Application of photocatalysts and LED light sources in drinking water treatment, *Catalysts* 3 (2013) 726–743.
- [24] L. Tang, L. Wang, H. Ou, Q. Li, J. Ye, H. Yin, Correlation among phenyltins molecular properties, degradation and cellular influences on *Bacillus thuringiensis* in the presence of biosurfactant, *Biochem. Eng. J.* 105 (2016) 71–79.
- [25] A. Taicheng, Y. Hai, S. Weihua, L. Guiying, L. Haiying, W.J. Cooper, Mechanistic considerations for the advanced oxidation treatment of fluoroquinolone pharmaceutical compounds using TiO₂ heterogeneous catalysis, *J. Phys. Chem. A* 114 (2010) 2569–2575.
- [26] M. Sturini, A. Speltini, F. Maraschi, L. Pretali, A. Profumo, E. Fasani, A. Albini, R. Migliavacca, E. Nucleo, Photodegradation of fluoroquinolones in surface water and antimicrobial activity of the photoproducts, *Water Res.* 46 (2012) 5575–5582.
- [27] X.X. Zhang, R. Li, M. Jia, S. Wang, Y. Huang, C. Chen, Degradation of ciprofloxacin in aqueous bismuth oxybromide (BiOBr) suspensions under visible light irradiation: a direct hole oxidation pathway, *Chem. Eng. J.* 274 (2015) 290–297.
- [28] T. An, H. Yang, G. Li, W. Song, W.J. Cooper, X. Nie, Kinetics and mechanism of advanced oxidation processes (AOPs) in degradation of ciprofloxacin in water, *Appl. Catal. B* 94 (2010) 288–294.
- [29] T. Paul, P.L. Miller, T.J. Strathmann, Visible-light-mediated TiO₂ photocatalysis of fluoroquinolone antibacterial agents, *Environ. Sci. Technol.* 41 (2007) 4720–4727.
- [30] G.S. Tillotson, Quinolones: structure–activity relationships and future predictions, *J. Med. Microbiol.* 44 (1996) 320–324.
- [31] Z. Ma, D.T. Chu, C.S. Cooper, Q. Li, A.K. Fung, S. Wang, L.L. Shen, R.K. Flamm, A. M. Nilius, J.D. Alder, Synthesis and antimicrobial activity of 4H-4-oxoquinolizine derivatives: consequences of structural modification at the C-8 position, *J. Med. Chem.* 42 (1999) 4202–4213.
- [32] B. Llorente, F. Leclerc, R. Cedergren, Using SAR and QSAR analysis to model the activity and structure of the quinolone–DNA complex, *Bioorg. Med. Chem.* 4 (1996) 61–71.
- [33] J.M. Domagala, Structure–activity and structure–side-effect relationships for the quinolone antibacterials, *J. Antimicrob. Chemother.* 33 (1994) 685–706.
- [34] X.X. He, A.A. de la Cruz, D.D. Dionysiou, Destruction of cyanobacterial toxin cylindrospermopsin by hydroxyl radicals and sulfate radicals using UV-254 nm activation of hydrogen peroxide, persulfate and peroxymonosulfate, *J. Photochem. Photobiol. A: Chem.* 251 (2013) 160–166.
- [35] C.Q. Tan, N.Y. Gao, S.Q. Zhou, Y.L. Xiao, Z.Z. Zhuang, Kinetic study of acetaminophen degradation by UV-based advanced oxidation processes, *Chem. Eng. J.* 253 (2014) 229–236.
- [36] C.Q. Tan, N.Y. Gao, Y. Deng, Y.J. Zhang, M.H. Sui, J. Deng, S.Q. Zhou, Degradation of antipyrine by UV, UV/H₂O₂ and UV/PS, *J. Hazard. Mater.* 260 (2013) 1008–1016.